

# Ultra-Wideband Radio Channel Characteristics for Near-Ground Swarm Robots Communication

Shihong Duan<sup>ID</sup>, Ran Su, Cheng Xu<sup>ID</sup>, Member, IEEE, Yulin Chen, and Jie He

**Abstract**—Ultra-Wideband (UWB) technology has great potential for the cooperation and navigation among near ground mobile robots in GPS-denied environments. In this paper, an efficient two-segment UWB radio channel model is proposed with considering the multi-path condition in very near-ground environments and different surface roughness. We conducted field measurements to collect channel information, with both transmitter and receiver antennas placed at different heights above the ground: 0cm-20cm. Signal frequency was chosen at 4.3GHz with bandwidth of 1GHz. Three ground coverings were tested in common scenarios: brick, grass and rubber fields. The proposed model has enhanced accuracy achieved by careful assessment of dominant propagation mechanisms in each segment, such as diffraction loss due to obstruction of the first Fresnel zone and higher-order waves produced by ground roughness. It is realized that antenna height and distance are the most influential geometric parameters to affect the path loss model. Once the antenna height is known, there exists a breakpoint distance in UWB propagation, which separates two segmentation using the different path-loss mechanism. Different surface types can cause different signal attenuation. Monte Carlo simulations are used to investigate the effects of antenna height, distance, ground surface type on mobile robots swarm communication to find out the antenna height is also a dominant factor on connectivity and the average number of neighbors. Within a certain range, the higher the antenna height and the closer the communication distance, the better the communication performance will usually be. Cramér-Rao lower bound(CRLB) of path loss estimator based on the proposed model is derived to show the relationship between CRLB with height and distance.

**Index Terms**—Near ground channel modeling, path loss, mobile robot network, multipath, Fresnel zone.

Manuscript received August 22, 2019; revised January 20, 2020 and March 30, 2020; accepted April 4, 2020. Date of publication April 14, 2020; date of current version July 10, 2020. This work is supported in part by National Natural Science Foundation of China project No. 61671056, No. 61971031, in part by the Post-doctoral Innovative Talent Support Program under Grant BX20190033, in part by Guangdong Basic and Applied Basic Research Foundation under Grant 2019A1515110325, in part by Postdoctor Research Foundation of Shunde Graduate School of University of Science and Technology Beijing under Grant 2020BH001, in part by the Fundamental Research Funds for the Central Universities under Grant 06500127 and in part by Scientific and Technological Innovation Foundation of Shunde Graduate School, USTB (No. BK19AF007). The associate editor coordinating the review of this article and approving it for publication was Z. Sun. (*Corresponding author: Cheng Xu*)

Shihong Duan, Ran Su, Yulin Chen, and Jie He are with the School of Computer and Communication Engineering, University of Science and Technology Beijing, Beijing 100083, China, and also with the Beijing Key Laboratory of Knowledge Engineering for Materials Science, Beijing 100083, China.

Cheng Xu is with the School of Computer and Communication Engineering, University of Science and Technology Beijing, Beijing 100083, China, also with the Beijing Key Laboratory of Knowledge Engineering for Materials Science, Beijing 100083, China, and also with the Shunde Graduate School, Institute of Artificial Intelligence, University of Science and Technology Beijing, Beijing 100083, China (e-mail: xucheng@ustb.edu.cn).

Color versions of one or more of the figures in this article are available online at <http://ieeexplore.ieee.org>.

Digital Object Identifier 10.1109/TWC.2020.2986446

## I. INTRODUCTION

MOBILE near-ground swarm robots with local sensing and communication capabilities have recently drawn the attention of the robotics community, especially situated in a possibly unknown environment performing collective actions [1]. Real-time and precise localization information of near-ground mobile robots is a key enabler for many emerging applications [2], [3]. In conventional systems, each robot individually determines its own positional states with either external measurement information, i.e., ranging distance to fixed infrastructures, or intra-measuring information using inertial sensors. Global navigation satellite system (GNSS) technology can provide meter-level positioning capability [4], [5]. While GNSS techniques become unreliable or even completely inaccessible in harsh or dense-constructed areas [1] due to signal blockage. Moreover, emerging applications of near ground robots in an unknown environment with no prior infrastructure may require a technology providing higher positioning accuracy than that of the current GNSS. The inertial-based technique is a potentially good solution in this case, but it still faces the problem of accumulative errors and drifting over time [24].

Correspondingly, Ultra-Wideband (UWB) technology characterized by the transmission of extremely short duration pulses, has become a competitive candidate technology for diverse ranging and positioning applications [6]–[10], which stands out in accurate ranging capability due to its ability to alleviate multi-path effects [8]. In particular, cooperative navigation proposed in [2] advocates that robots jointly use both spatial and temporal cooperation for real-time localization shown as in Fig. 1. In the spatial domain, each robot obtains  $info_{ij}^n$  ( $j \neq i$ ) defined as a collection of  $\{ChannelInfo_{ij}^n, distance_{ij}^n, data_{ij}^n\}$  by inter-node measurement. In the temporal domain, each robot obtains  $info_{ik}^n$  by intra-node measurements. Thus, it is important to maintain precise and reliable communication channel states for inter-nodes information exchange.

Knowing the channel characteristics of UWB in near-ground scenarios is the premise and basis of getting precise  $ChannelInfo_{ij}^n$ , correcting the ranging error and designing computationally efficient and reliable robots network topology. Mobile robots used in military, agriculture monitoring, and landslides monitoring are often operated at the ground-level with the antenna height less than 20 cm [9], [25]–[27]. Most of the few existing models proposed in the literature for the near-ground channel are incomplete and become specific to the considered scenario, frequency bands, antenna height, and terrain roughness, etc.. Near-ground channel models and experimental results reported in typical works of literature are

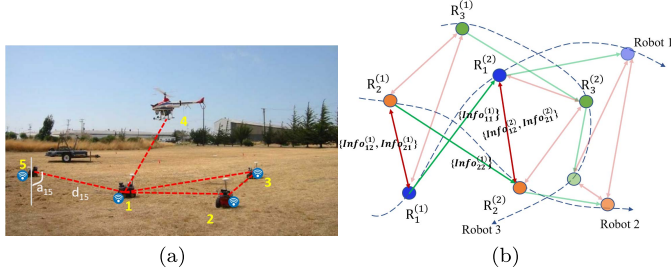


Fig. 1. Near-ground mobile robots network swarm. (a) A sketch of typical near-ground navigation scenario. (b) Three mobile robots (circles with different colors), in three different time steps  $(R_{i=1-3})^{(1)}, (R_{i=1-3})^{(2)}, \dots$ , aiming to locate their own spatial status by using inter-node measurements  $\{\text{Info}_{kj}^{(n)}\}$  (red arrows) describing information from robot  $k$  to  $j$  in time step  $n$ , and intra-robot measurements  $\{\text{Info}_{kk}^{(n)}\}$  (green arrows) describing the information achieved in time step  $n$ .

briefly described as follows, showing RF signal bandwidth and working frequency, specific measurement scenario, scope and validation.

The characteristics of wireless channels, such as channel impulse response, power delay profile, the number of paths, Doppler spectrum, path loss exponent and shadowing parameters for near-ground wireless communication were preliminarily statistically analyzed based on field measurement in [10]–[13]. Channel models always were based on measurement campaigns, simulations, or just derived as mathematical models.

Narrowband wireless path-loss characteristics attracted more researchers. [10] presented the theoretical three-segment path-loss model validated by narrow-band signals at the frequency of 300MHz, which facilitated highly accurate WSN simulation, with consideration of the impact of first Fresnel zone obstruction, higher-order waves and etc. [16]–[18] focused on analysis of path-loss in narrow-band channel analysis, based on outdoor measurement at different frequency; but no model was proposed, only the influence factors on channel variance was discussed. [14] completed outdoor measurement of narrow-band with the frequency of 868MHz, 2.4GHz and 5.8GHz, the TX and RX antennas were placed from 1m to 25m apart, at height of 0.2m and 0.4m, and three ground coverings were tested in a rural scenario: soil, short and tall grass fields. [14] tailored a three-slope log-normal path loss model, and compared the path loss results with different combinations of antenna heights, frequency bands, and ground coverings to confirm the obstruction of First Fresnel Zone. [19]–[21] proposed channel variance for WSN based on simulation which has limited scalability and only valid for certain environments.

However, quite a few fundamental questions of UWB propagation are not yet answered in a satisfactory way, especially in near-ground environment [15]. Near ground UWB wireless channels were always deducted as typical log-normal models with statistical distribution parameters proposed in [11]–[13]. [11] carried out indoor UWB radio propagation measurement from 0.2GHz to 12GHz, the antennas with the height of 0m – 1m were placed on a concrete floor covered by either

tile or carpet, and the distance between transmitter (Tx) and receiver (Rx) was 2m. [11] concluded that lowering the antennas shrinks the range of the entire system, significantly decreases the amount of receive power, increases the shadowing variance. [12] performed outdoor UWB measurements from 3GHz to 10GHz in rural flat and hilly terrains during the rainy season, the antennas of Tx and Rx were placed in 5m to 200m apart, at the height of 10cm to 200cm. [12] found that the path loss coefficients increase significantly as the transmitter and receiver get closer to the ground. [13] developed air-to-ground propagation channel models and analyzed the channel multipath characteristics based on UWB outdoor measurements from 3.1GHz to 5.3GHz by using one UAV transmitter at the height of 4m to 16m, and three receivers at the height of 1.5m and 7cm.

Based on analysis of near-ground radio channel models and experimental results in above literatures, the following conclusions could be drawn:

- 1) Near-ground application scenarios have been becoming more and more common in various applications, especially in military, agriculture and environment detection with robots. For example, the Self-Healing Minefield system in [9] had an antenna phase-center height of 7cm above the ground. But WSNs working on narrow-band are research hot issues [10], [14]–[16], [18], [20], [21], very near-ground UWB channel analysis is generally ignored. Some related researches on UWB channels focused on antenna height around 1m [11], [12], and others focused on air to ground signal transmission path loss [13].
- 2) Existing studies mostly focused on narrow-band RF propagation link in near-ground scenarios. UWB channel model is different from that of narrow-band, because the bandwidth difference may cause different attenuation conditions. UWB propagation modeling is interesting mainly for the 3–5 GHz range when immediate commercial applications are considered from [15]. However, quantitative models showing the near-ground influence factors on UWB wireless channel with 3-5GHz working frequency are seldom analyzed.
- 3) There is a lack of theoretical analysis on the influencing factors of near-ground UWB channel model. Literatures [10] and [14] took the influence of the first Fresnel zone into consideration and deduced the three segmentation models by statistical or theoretical derivation. However, they were not validated by UWB measurements. Ground surface roughness generates incoherent scattering, as known as diffuse scattering [21]. Incident signals are scattered in multiple directions to weaken the signal energy, degrade the accessible range and connectivity [10].

Based on the above analysis, in this paper, we focused on modeling near-ground UWB channel characteristics. The influencing factors of near-ground UWB channel are analyzed in detail, including communication distance, antenna height, and ground-surface conditions, etc. The theory of Fresnel zone [10], [28] is taken into consideration of building near-ground

UWB channel models. The main contributions of this paper could be summarized as follows:

- A field-measurements-based UWB radio channel model is proposed to predict path-loss for near-ground robots navigation. Typical influence factors are taken into consideration, including communication distance, antenna height, and ground surface conditions. A comprehensive measurement campaign was carried out for 3.1-5.3 GHz UWB spectrum in outdoor areas with three types of the ground surface, namely brick floor, rubber, short grass.
- The principle of Fresnel zones [28] is exploited to split the proposed path-loss model into two segments. The factors affecting channel fading in near-ground scenarios are analyzed in detail. Then, the channel model parameterized based on practical measurements is used to verify the theoretical analysis.
- The proposed near-ground UWB channel model is verified from both practical and theoretical aspects. Practically, path-loss predictions offered by our proposed model are consistent with the measurement results. Theoretically, the CRLB of path-loss estimation is calculated and analyzed based on the proposed model. Moreover, in order to verify the effectiveness of the proposed path-loss model, we examine the influence of coverage range and network connectivity in near ground robots networks by exploring Monte Carlo simulations.

The rest of this paper is organized as follows. The measurement and multipath condition of near-ground UWB channel characteristics are introduced in Section II. In Section III, the near-ground segmented path-loss model is developed. The proposed models are verified in Section IV. They are employed in mobile robots connectivity analysis and utilized in the derivation of Cramér-Rao lower bound for path-loss estimation. Section V concludes the paper.

## II. MULTIPATH CONDITION OF NEAR-GROUND UWB CHANNEL BETWEEN ROBOT PAIRS

In this section, we will firstly present the process of channel sounding method with P440 UWB kits [13], [22], and then illustrate the multipath condition of near-ground UWB channel for communication between robot pairs. Theoretical analysis of dominant influence factors on channel attenuation related to near-ground conditions is closely elaborated.

### A. Channel Sounding With P440 Kits

For UWB measurement campaigns to determine the impulse response of the channel, Time Domain P440 UWB radios are used to work in bi-static mode [31]. Transmitter radio sounds the channel by sending a short duration pulse similar to a Gaussian shape in the time domain at regular intervals of time. The transmitted pulse repetition rate is 10.1 MHz. There is no need for physical synchronization between the transmitter and the receiver. The frequency of operation for the P440 UWB kits is from 3.1 GHz to 5.3 GHz with an operational center frequency of 4.3 GHz. The maximum transmit power is limited to 0.71 dBm.

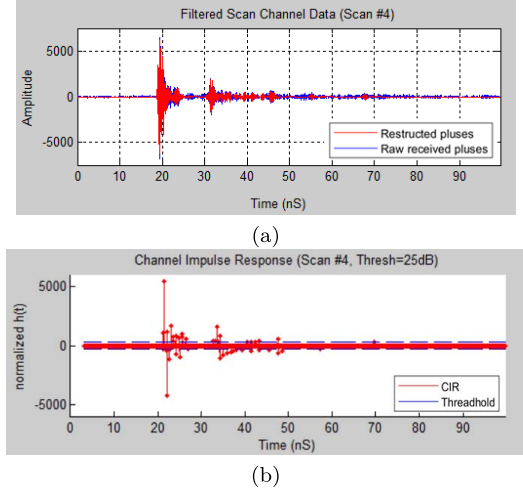


Fig. 2. Channel data at receiver. (a) Amplitude of received pulse and reconstructed pulse, (b) Normalized CIR.

A rake receiver is used with a delay bin resolution of 1.9073 ps for collection of Multipath Components (MPCs). A standard 32 bin duration is maintained between two measurements, and each measurement sample is processed after 61 ps. Original amplitude of the received raw pulses is shown in Fig. 2-(a) in blue. Clean algorithm [20] is used for obtaining refined channel impulse response (CIR) in Fig. 2-(b) by deconvolving the received pulses with the template waveform. The CIR in Fig. 2-(b) is obtained by the dashed blue horizontal lines indicate the amplitude threshold of the MPCs selected at 20% of the input signal, where all CIR samples below the threshold are discarded. At last, the reconstructed pulses shown in red are obtained by convolving the CIR shown in Fig. 2-(a) with the template waveform. The difference between raw Rx and reconstructed Rx is due to the imperfection of the clean algorithm.

The received signal in time domain can be demonstrated as:

$$r_t = \sum_{n=1}^N a_n x(t - \tau_n) + n(t) \quad (1)$$

where  $N$  is the number of multipath components (MPCs) between Tx and Rx,  $a_n$  is the received amplitude of the  $n$ th arriving path,  $x(t - \tau_n)$  is the waveform at the time of  $\tau_n$ , and  $n(t)$  is the received additive noise. Then, CIR can be expressed as:

$$h(t) = \sum_{n=1}^N a_n \delta(t - \tau_n) \quad (2)$$

where  $a_n$  is the channel gain got by received antenna,  $\tau_n$  is the pulse delay of the  $n$ th path, and  $\delta(t)$  corresponds to the Dirac function.

### B. Multipath Conditions Analysis of Near-Ground UWB Channel

The corresponding terminology of various wave components involved in ground-wave propagation is defined in the standard 211-1997 [8]. As shown in Fig. 3, [32] and [33]

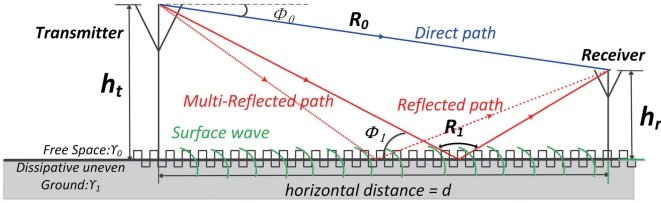


Fig. 3. Multipath condition of near-ground wireless channel [24], [32], [33]: A sketch of typical near-ground scenario. Tx and Rx antennas are put on top of a dielectric half-space, showing direct waves, ground-reflected waves and surface waves.

presented near-ground propagation process, involving three kinds of waves directed wave, ground reflected wave and ground surface wave.

For a dipole antenna located at  $h$  above the ground, the generated magnitude of the electric field could be demonstrated as in [33]:

$$E_{total} = \frac{E_0}{d} \left[ \underbrace{\cos^3(\phi_0) e^{-\gamma_0 R_0}}_{\text{Direct Wave}} + \underbrace{\Gamma_{v,h} \cos^3(\phi_1) e^{-\gamma_0 R_1}}_{\text{Ground-reflected Wave}} + \underbrace{(1 - \Gamma_{v,h}) F(w) \cos^2(\phi_1) e^{-\gamma_0 R_1}}_{\text{Surface wave}} \right] \quad (3)$$

where  $E_0$  is a reference value representing the excitation and  $\Gamma_{v,h}$  is the Fresnel plane-wave reflection coefficient of the boundary between the free space and the dissipative ground for vertical and horizontal antenna polarization.  $\gamma_0$  is upper half-space (air) propagation constant( $meters^{-1}$ ) in dielectric medium of free space.  $F(w)$  denotes the Sommerfeld attenuation function.  $R_0$ ,  $R_1$ ,  $\phi_0$ ,  $\phi_1$  and  $h$  is defined in Fig. 3.

$$R_0 = \sqrt{d^2 + (h_t - h_r)^2} \quad (4)$$

$$R_1 = \frac{h_t + h_r}{\sin \phi_0} \quad (5)$$

$$\cos(\phi_0) = \frac{h_t + h_r}{d} \quad (6)$$

The complex propagation constant of the medium is denoted by  $\gamma = (-\omega^2 \epsilon \mu + j \omega \mu \sigma)^{1/2}$  and the corresponding time factor is  $\exp(j\omega t)$ .  $\omega$  is angular frequency,  $\epsilon$  is the dielectric constant of the ground referred to air as unity,  $\sigma$  is the conductivity of the ground measured in electromagnetic units, and  $\mu$  is permeability of free space.

$$\Gamma_{v,h} \propto \frac{h_t + h_r}{R_1} \quad (7)$$

$F(w)$  corresponds to elevated transmitting and receiving antennas, namely

$$F(w) = [1 - j \sqrt{\pi w} e^{-w} \operatorname{erfc}(-j \sqrt{w})] \quad (8)$$

where the numerical distance  $w$  is

$$w \simeq -\frac{\gamma_0 R_0}{2} \sin(\phi_1 + \frac{\gamma_0}{\gamma_1})^2 \quad (9)$$

By taking a closer look at how (3) is derived, we conclude that in near-ground propagation scenario, received pulses are significantly related with antenna heights of both sides ( $h_t$  and  $h_r$ ), Tx-Rx distance( $d$ ), and the frequency. For better

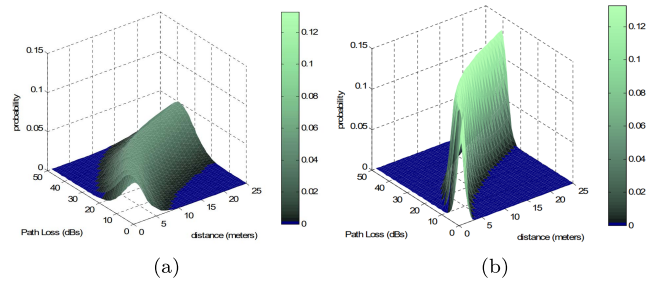


Fig. 4. Probability distribution function [35] (a) for conventional channels, (b) for UWB channels.

estimation of signal loss in near ground wave propagation, a field measurement study is needed to cover all these factors.

*1) Difference Between UWB and Conventional Channels:* Works of literature related to near-ground channel characteristics often focused on conventional (narrow-band) scenarios. While delay variation of UWB channel increases compared with the conventional channel, meanwhile amplitude variation decreases, so conventional channel measurements and modeling cannot be reused in UWB channel. Molisch gave the conclusion in [15] that one of the key differences between UWB propagation channels and conventional channels lies in the frequency dependence of the transfer function. Different frequency components will cause different reflection/diffraction coefficients of obstacles. The distance dependence of the path gain is the same as that of most narrow-band channel models. [35] presented that shadowing parameter is different between the conventional and UWB channels, with a much larger shadowing variance seen in the conventional model, as shown in Fig. 4.

*2) Influence of Fresnel Zone on Near-Ground Channels:* Path-loss caused by near-ground can be explained further in terms of Fresnel zone [10]. The Fresnel zones around a communication link are ellipsoids with their **foci** at the Tx and the Rx, the axis of symmetry coincides with the line connecting Tx and Rx. The locus of all points in the  $n$ th ellipsoids have a constant value of excess path length  $\Delta d_n$ , and  $\Delta d_n$  varies in integer multiples of half-wavelength, that is  $\Delta d_n = \frac{n\lambda}{2}$ . The intersection of these Fresnel ellipsoids with an imaginary plane perpendicular to the LOS path constructs a family of concentric circles with radii  $r_n$  by using  $d_1$ ,  $d_2$  defined in Fig. 5.  $d_b^h$  is the break distance as the minimum distance for which the condition for the existence of near-ground path-loss (that is based on 60% of the first Fresnel radius  $r_n$  and  $r_1$ ) is satisfied. It is assumed that the antenna height of the transmitter and the receiver are the same, denoted by  $h$ .

From Fig. 5, we can conclude that when  $d_1 + d_2 < d_b^h$ , direct wave from Tx to Rx is the dominant transmission signal; while when  $d_1 + d_2 \geq d_b^h$ , the multipath influence of diffraction wave and reflection wave on path loss can not be omitted. The definition of  $r_n$  and  $d_b^h$  is shown in Equation (10).

$$r_n = \sqrt{\frac{n \lambda d_1 d_2}{d_1 + d_2}}$$

$$d_b^h = \frac{h^2}{0.09 \lambda} \quad (10)$$

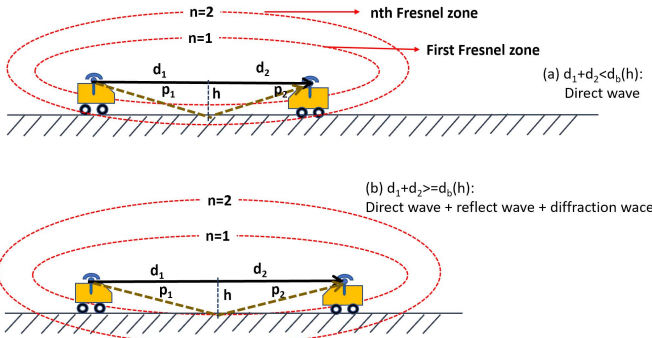


Fig. 5. Schematic representation of the first Fresnel zone in a radio link depends on the geometry of the receiver, transmitter and ground.

**3) Influence of Surface Roughness on Near Ground Channels:** In general, a surface is called rough if the variation of the height of roughness,  $\Delta h$ , is in the order of the transmission wavelength,  $\lambda$ . More specifically, the ground is considered rough if

$$\Delta h > \frac{\lambda}{32} \quad (11)$$

Usually, the heights of the ground in different positions are correlated with the correlation distance  $L_C$ , with the coefficient of

$$C_h(l) = e^{l^2/L_C^2} \quad (12)$$

Here,  $L_C$  represents the distance of two points on the ground, for which the heights of antennas are highly correlated. If  $\Delta h$  is high,  $L_C$  should be very small (or  $L_C \rightarrow 0$ ). If  $\Delta h$  is low,  $L_C$  would be very large (or  $L_C \rightarrow \infty$ ). Thus, the ground surface is rough if  $L_C < 5\lambda$ .

In our research, the central frequency of UWB radio is 4.3GHz, so  $\lambda$  is about 7cm,  $\Delta h$  is about 2.2mm, and  $L_C$  is about 35cm. Any point of the rough surface scatters the incident wave into various directions with a certain probability. According to the Kirchhoff theory [28], reflection by a rough surface shows a strong dependence on the considered frequency, and the reflection coefficient for the specular component  $\rho$  is

$$\rho_{rough}(f) = \rho_{smooth} \exp[-2(2\pi \frac{f}{c_0} \sigma_h \sin \psi_0)^2] \quad (13)$$

where  $\sigma_h$  is the standard deviation of the height distribution,  $\psi_0$  is the angle of incidence, and  $\rho_{smooth}$  is the reflection coefficient that would occur if the surface were smooth. Based on the analysis of the reflection coefficient from a rough surface, the influence of surface roughness on channel characteristics should be covered. In our channel measurement in UWB near ground communication scenario, the ground surface type is considered as one of influence factors.

Above all, we can conclude that near-ground UWB channel path-loss is largely affected by the following factors: communication distance, antenna height, and ground surface conditions. In the following section, we would present a field-measurements-based UWB channel model with all the above-mentioned factors taken into consideration.

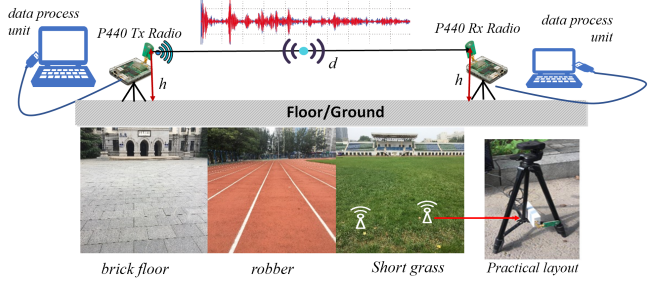


Fig. 6. Experimental setup for near-ground propagation measurements using P440 kits on three different surface types  $ST = \{b : \text{brick}, r : \text{rubber}, sg : \text{shortgrass}\}$  at University of Science and Technology Beijing.

### III. NEAR GROUND CHANNEL MEASUREMENT AND MODELING

By field measurement in actual outdoor near ground scenarios, statistical measurements are conducted to quantitatively analyze the effects of antenna height, Tx-Rx distance, and ground surface type on channel path-loss. In this section, Experiment setup is described firstly, then the empirical UWB channel model is investigated according to our near-ground channel sampling dataset, and finally a two-segmented channel model related to geometric optics and Fresnel zone concepts.

#### A. Measurement Layout and Scenario

Measurement platform conducted using Time Domain P440 UWB radios module is shown in Fig.6, and the radios work in bi-static mode. Transmitter and receiver are connected respectively with a laptop by USB interface, the antennas used in measurement are BroadSpec UWB planar elliptical dipole antennas. The amplitude response of the antennas over the band is approximately flat.

We put the P440 with omni-antenna on the tripod, and the antennas are perpendicular to the ground and face to face. The beam pattern in the azimuth plane is in the form of circles spreading outward to provide optimum coverage. The measurement case set is denoted by:  $Case = \{h, d, ST\}$ , where subset  $h = \{6cm, 8cm, 10cm, 12cm, 14cm, 16cm, 18cm, 20cm\}$  is the antenna height of Tx and Rx, subset  $d = \{1m, 2m, 3m, 4m, 5m, 6m, 8m, 10m, 16m, 20m\}$  is the distance between Tx and Rx, and  $ST = \{b, r, sg\}$  describes the surface types: brick ground, rubber ground, and short grass ground.  $\{h, d\}$  are adjusted by change the tripods height with a ruler, and the distance  $d$  between the tripods measured by using P440 ranging module RET [30].

In order to guarantee accuracy and validity of measurement and channel modeling,  $N_s \geq 500$  snapshots are obtained in each measurement case, and the number of frequency sample points in each snapshot is denoted by  $N_f = 1632$ . The original data in one case is a two-dimensional array of  $N_s * N_f$ , and in total 120,000 measurement data samples are collected and uploaded to the web disk [23], which is opened to the public researchers to reuse our dataset.

Based on measured data, received signal energy ( $P_r$ ) at the Rx, and propagation loss (PL) can be denoted by

TABLE I  
PATH LOSS EXPONENT AND STANDARD DEVIATION OF RANDOM SHADOW VARIATION WITH DIFFERENT ANTENNA HEIGHT

$h(\text{cm})$	6	8	10	12	14	16	18	20
$N_{first}$	3.1105	3.0572	2.8998	2.9118	2.2086	1.9828	2.6166	2.1676
$N_{total}$	3.1260	2.8647	2.5043	2.6013	2.3751	2.1940	2.4680	2.2086
$\sigma_{first}$	0.7795	0.4290	0.4907	0.4176	0.3213	0.3860	0.7669	0.2924
$\sigma_{total}$	0.4210	0.3398	0.2947	0.2399	0.2441	0.2847	0.4302	0.21510

Equation (14):

$$P_r = \sum_{n=1}^M |h[n]|^2$$

$$PL(dB) = 10 \log \frac{P_t}{P_r} \quad (14)$$

where  $P_t$ ,  $P_r$  are transmitting power and received power respectively,  $h[n]$  describes the CIR value of the  $n$ th path.  $M$  means the number of samples in the generated fading impulse response. When  $M = 1$ ,  $h[n]$  corresponds to the impulse signal value of the first path, and  $P_r$  is the first path received power; when  $M > 1$ , the calculated  $P_r$  is the total received power.

### B. Parameterization of Empirical Statistical Channel Model

In this section, we first discuss the propagation characteristic of the near-ground UWB channel based on the slow fading model, which is the superposition of path loss and random shadow variation. Typical log-normal distance path loss model is generic to be used for predicting the propagation loss for a wide range of environments. The path loss is the average of the signal attenuation related to the distance  $d$  between the Tx and Rx, with path loss exponent related to different environments. Shadowing effect on channels is described by a zero-mean Gaussian distributed random variable (in dB) with standard deviation( $\sigma$ ), which can produce signal fluctuation. Therefore, the first path loss model and the total path loss model can be given by Equation (15).

$$PL(d) = PL(d_0) + 10N \log_{10} \frac{d}{d_0} + X_\sigma$$

$$X_\sigma = G(0, \sigma) \quad (15)$$

where  $PL(d)$  is path-loss in dB at an arbitrary distance  $d$ .  $PL(d_0)$  is path loss in dB at the distance  $d_0$ .  $N$  is path-loss exponent for modeling the slope.  $X_\sigma$  is random shadow variation meeting Gaussian distribution with different standard deviation  $\sigma$ .  $N$  and  $X_\sigma$  are all related to various environmental factors. The least squares method is employed to estimate  $N$  and  $X_\sigma$ , that is minimizing the sum of the squared deviations of the measured path loss from the estimated path loss given by the statistical fitting formula. Fig. 7 shows the fitting results of the first path-loss and total path-loss with different antenna heights and distances on the brick floor.

From Fig.7, we can see antenna height is a major factor to affect path loss in the near-ground application scenario. The lower the antenna is, the greater the slope of the fitting curve

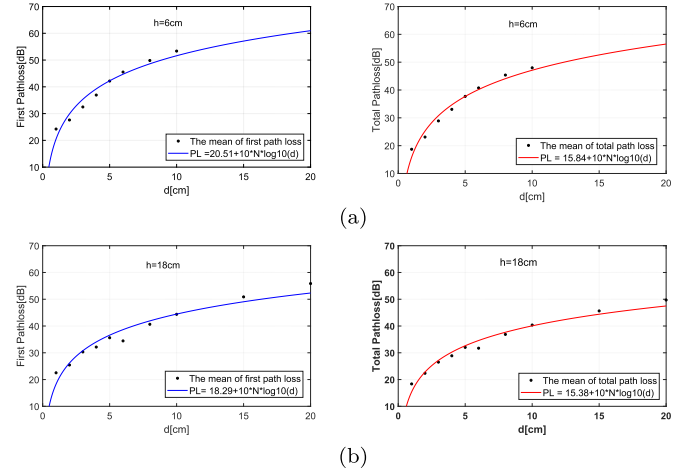


Fig. 7. First pathloss and total pathloss. (7a):  $h = 6\text{cm}$ , (7b):  $h = 18\text{cm}$ .

is, and the bigger  $N$  is. The least-squares fitting method is applied and the fitting result is presented as Equation (16).  $PL_{first}$  and  $PL_{total}$  are defined as path loss of first path and total path,  $N_{first}$  and  $N_{total}$  are path loss exponent of first path and total path. We use the least-squares fitting method to get the relationship between  $\sigma$  and antenna height, which is described by Equation (17). The optimal fitting values of  $N_{first}$  and  $N_{total}$ ,  $\sigma_{first}$  and  $\sigma_{total}$  with different antenna height are shown in Table I. A linear logarithmic relationship exists between path-loss exponent and antenna height. From analyzing sampling data, we found the random shadow variation  $X_\sigma$  obey Gaussian distribution with different standard deviation  $\sigma$  because of different antenna height. The optimal fitting values of  $N_{first}$  and  $N_{total}$ ,  $\sigma_{first}$  and  $\sigma_{total}$  with different antenna height are shown in Table I.

$$PL_{first}(d) = PL_{first}(d_0) + 10N_{first} \log_{10} \frac{d}{d_0} + X_{\sigma_{first}}$$

$$N_{first} = -1.9945 * \log_{10}(h) + 0.791$$

$$\sigma_{first} = -0.4195 * \log_{10}(h) + 0.1009 \quad (16)$$

$$PL_{total}(d) = PL_{total}(d_0) + 10N_{total} \log_{10} \frac{d}{d_0} + X_{\sigma_{total}}$$

$$N_{total} = -1.6280 * \log_{10}(h) + 1.0504$$

$$\sigma_{total} = -0.1967 * \log_{10}(h) + 0.1284 \quad (17)$$

Empirical log-normal shadow path-loss model described in this section is deducted by statical methods. Parameters of the model, including  $N$  and  $\sigma$ , are all function of  $h$ . But from Fig. 7, we can conclude that there exists the deviation between

the measured data and the model, also there is an inflection point unable to be described in the logarithmic model function. Especially, the higher the antenna height, the more obvious the deviation and inflection points. The influence of Fresnel zone on the signal transmission will be considered in the next subsection to improve model accuracy.

### C. Fresnel Zone Based UWB Near Ground Path-Loss Model

In near-ground scenarios for data exchange between robots, interference owing to the direct and geometrical-optics reflection is different obviously to give different power falloff. When  $d_h < d_b^h$ , the first Fresnel zone is free of obstacle. In this region, direct signal transmission is the dominant propagation mechanism. The attenuation of the median received signal with distance corresponds to the free-space path loss (denoted as  $PL_f$ ).

When  $d_h \geq d_b^h$ , part of the energy in the first Fresnel zone is intercepted by the ground. Therefore, attenuation results from both spherical wavefront spreading and obstruction of the first Fresnel zone, which lead to a more pronounced decay rate. The knife-edge diffraction model [10] is generally used to find the loss due to the influence by the first Fresnel zone principle. Path-loss model used in this section is based on this idea that the diffraction loss (denoted as  $PL_{NG}$ ) due to the non-knife edge is equal to the sum of ideal knife-edge approximation (denoted as  $PL_{ke}$ ) and an additional loss (denoted as  $PL_{Ad}$ ).

According to Fresnel zone and transmit wave composition theory [9], [10], the near-ground path-loss  $PL$  is defined as two-segmentation model shown in Equation (18). The critical distance  $d_b^h$  decides different dominant influence factors on different channel fading principles. In the first region, the LOS ray free fading mechanism dominates the signal transmission. In the second region, both the direct and ground-reflected signals impact the received energy, so the sum of free-space path loss ( $PL_f$ ) and near-ground diffraction loss ( $PL_{NG}$ ) can account for the influence of the first Fresnel zone obstructed by the ground.

$$PL = \begin{cases} PL_f & d_h < d_b^h \\ PL_f + PL_{NG} & d_h \geq d_b^h \end{cases} \quad (18)$$

We compared sampling path-loss data shown as asterisk points with generated data shown with green curve generated by the model defined in Equation (18). There exists a deviation  $N_C$ , as shown in Fig.8. Deviation  $N_C$  is different with different antenna heights ( $h$ ) and different surface types in our data analysis.  $N_{C_{first}}$  and  $N_{C_{total}}$  is respectively the deviation of the  $PL_{first}$  and  $PL_{total}$ , so the Fresnel-zone-based two-segmentation model is expressed in Equation (19). When the antenna height is relatively low, the two-segmented model corrected by  $N_C$  is not significantly better than the empirical log-normal shadow path-loss model. However, when the antenna height is higher, the two-segmentation model shows more advantages, which are summarized and displayed in Fig. 8-(b).

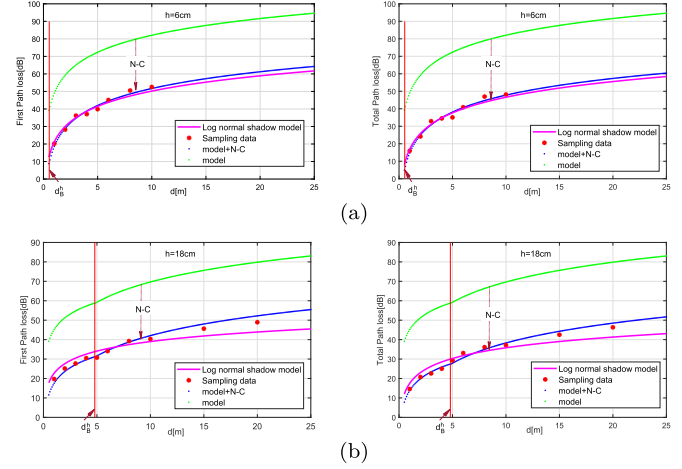


Fig. 8. Comparison of pathloss model with deviation  $N_C$  and sampling data point in our measurement. (8a):  $h = 6\text{cm}$ ,  $d_B^h = 0.5940\text{m}$ , (8b):  $h = 18\text{cm}$ ,  $d_B^h = 4.6940\text{m}$ .

The corrected two-segmented path-loss model using  $N_C$  is demonstrated with Equation (19).

$$PL = -N_C + \begin{cases} PL_f & d_h < d_b^h \\ PL_f + PL_{NG} & d_h \geq d_b^h \end{cases} \quad (19)$$

$$PL_f = 32.44 + 20 \log_{10}(f \times 10^{-6}) + 20 \log_{10}(d \times 10^{-3}) \quad (20)$$

$$PL_{NG} = PL_{ke} + PL_{Ad}$$

$$PL_{ke} = -20 \log_{10}(0.5 + \frac{1.75h}{\sqrt{d\lambda}})$$

$$PL_{Ad} = K \times \frac{1}{(100h^2)/9d\lambda}, \quad K = \ln(10) \quad (21)$$

$$PL_{NG} = -20 \log_{10}(\frac{5h}{3\sqrt{d\lambda}} + \frac{35h^2}{6\sqrt{d\lambda}}) \quad (21)$$

$$N_C = ah^4 + bh^3 + ch^2 + dh + e \quad (22)$$

$N_{C_{first}}$  and  $N_{C_{total}}$  on different  $ST$  is shown in Table II by statistical analysis.  $N_C$  values depend on different surface types and antenna heights. Thus, we use the least-squares method to fit the function of the antenna height. The curve equation is assumed to be n-order polynomial. The first-order curve to the fourth-order curve are tried, and the fitting results are shown in Fig.9. The fourth-order polynomial function can best match the  $N_C$  variances according to the measurement data on all three-type grounds.

$N_C$  is different in different ground-surface conditions, and the relationship is calculated by fitting statistics methods, which is demonstrated in Table II. Based on the statistics and analysis, the deviation of  $N_C$  is considered as the comprehensive result of near ground factors, mainly related to the surface conditions.

#### IV. MODEL VALIDATION AND TYPICAL USE CASES

In this section, we validate the proposed path-loss model from both practical and theoretical aspects. Practically, the prediction ability of the proposed model is verified by comparing it with the parameterized empirical log-normal path-loss

TABLE II  
 $N_C$  VALUES WITH DIFFERENT GROUND SURFACE AND ANTENNA HEIGHTS

<i>ST</i>	<i>h(cm)</i>	6	8	10	12	14	16	18	20
brick	$N_{C_{first}}$	29.83	30.11	30.65	27.37	31.57	32.94	24.88	30.41
	$N_{C_{total}}$	34.40	34.79	35.63	33.22	36.25	35.89	28.86	33.28
	$N_{C_{first\_brick}} = 275380h^4 - 142670h^3 + 26180h^2 - 2001.81h + 83.4067$								
$N_{C_{total\_brick}} = 260024h^4 - 133440h^3 + 23973h^2 - 1778.62h + 80.5880$									
rubber	$N_{C_{first}}$	25.63	29.42	23.72	25.08	31.49	29.30	27.58	30.38
	$N_{C_{total}}$	29.97	32.99	28.62	29.39	34.46	33.67	30.91	33.86
	$N_{C_{first\_rubber}} = 6342.3h^4 - 8302.9h^3 + 2669h^2 - 282.15h + 35.6249$								
$N_{C_{total\_rubber}} = 6342.3^4 - 15856h^3 + 3834.8h^2 - 355.52h + 41.4221$									
grass	$N_{C_{first}}$	30.37	31.67	28.38	25.49	29.46	27.16	27.59	28.40
	$N_{C_{total}}$	34.25	35.28	32.19	29.29	32.92	31.21	31.35	31.32
	$N_{C_{first\_grass}} = -184060^4 + 96729h^3 - 17684h^2 + 1287.2h - 1.3166$								
$N_{C_{total\_grass}} = -222140^4 + 113940h^3 - 20410h^2 + 1464.65h - 1.5367$									

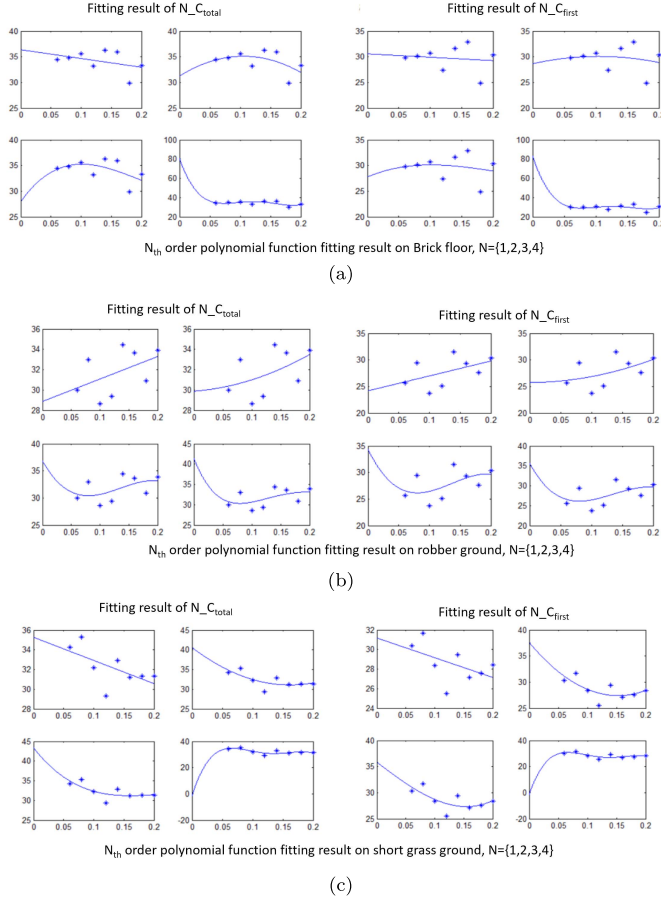


Fig. 9. Fitting function result of  $N_C$  on different ground surface. (a): on brick floor, (b): on rubber ground, (c): on short grass ground.

model, and field-measured data samples in near-ground conditions are used for verification. Theoretically, the influence of ground roughness and geometrical properties on the connectivity of low-altitude mobile robots network is investigated, and at last CRLB is derived for performance estimation via Monte-Carlo simulation.

#### A. Model Validation and Comparison Experiment

Over 500 snapshots are obtained in each measurement case stated in Section II. Among them, 400 snapshots are used to build the channel model, and the other 100 snapshots are used for verification. Predicted path-loss data by the parameterized empirical model and the two-segmentation model are compared with measured data. The results show a high degree of coincidence of test data and model data, which indicates that two-segmentation model has credibility and good predictability.

Mean squared error (MSE) is used as an evaluation indicator to assess the accuracy of the proposed channel model. For comparison, the MSE of the log-normal distribution model and proposed two-segmented model are both calculated. For each sampled case ( $h, d, ST$ ), the predicted value of each model could be calculated by substituting parameters into the model. Then, compared with sampling data, MSE could be obtained as:

$$MSE = \frac{1}{M} \sum_{t=1}^M (sampling_t - predicted_t)^2 \quad (23)$$

where  $sampling_t$  and  $predicted_t$  are respectively the  $t_{th}$  sampling data and estimated value calculated by channel model.  $M$  is the number of the data for verification. The MSE of above-mentioned two models are listed in Table III.

From Table III we can see that MSE of the two-segmentation model is generally smaller than that of traditional log-normal shadowing model. Thus, the two-segmentation model shows more accurate performance, which is possible because the proposed model takes more consideration about diffraction effects caused by the terrain roughness and geometry optics owing to Fresnel zone mechanism. Besides, there is a critical value of  $d_b^h$  related to antenna height, which can separate the channel characteristics with different dominant path-loss influence factors. The higher the height of the antenna, the bigger the  $d_b^h$ , and the easier the effects of the Fresnel zone mechanism could be seen.

TABLE III  
MSE OF THE CHANNEL MODEL WITH MEASUREMENT DATA

	h(cm)	6	8	10	12	14	16	18	20
lognormal model	$MSE_{brick}$	8.63	14.92	27.67	10.27	24.41	31.37	15.84	7.97
	$MSE_{robbert}$	5.32	22.12	9.43	22.94	25.71	33.15	34.51	20.23
	$MSE_{grass}$	9.03	18.96	26.56	10.7	26.22	41.24	21.04	325.88
two-segment model	$MSE_{brick}$	3.46	7.07	10.17	8.70	10.18	13.81	10.55	3.96
	$MSE_{robbert}$	2.57	12.43	6.19	6.17	11.42	5.49	12.22	4.57
	$MSE_{grass}$	4.54	16.29	19.19	8.94	17.23	17.04	18.57	11.30

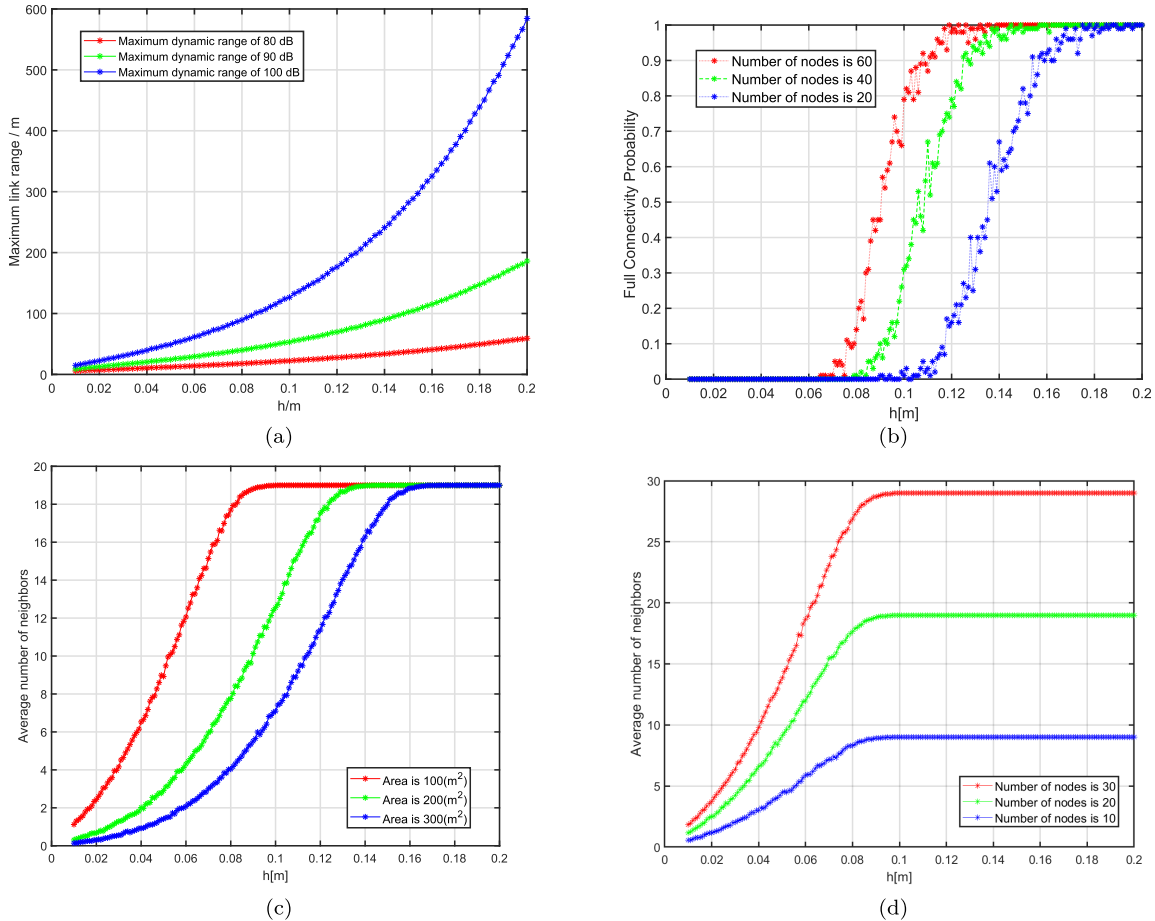


Fig. 10. Simulation robots network parameters analysis based on UWB channel mode, including link range, connectivity and number of neighbors. (a) Robot nodes transmission range versus different maximum dynamic range at different antenna height. (b) Full connectivity probability versus the number of nodes number with different antenna height. (c) The average number of neighbors versus different plane size at different antenna height. (d) The average number of neighbors versus the number of nodes at different antenna height.

### B. Model Application in Robot Network Navigation

In this section, our proposed two-segmentation path-loss model is validated in mobile robots network applications. Significant characteristics, including the maximum transmission range, network connectivity, and coverage, are considered via Monte Carlo simulations. All these factors are critical in node deployment to guarantee the optimum node density, the quality of service (QoS), scalability, and reliability.

The simulation scenario is set up as follows: The maximum transmission power of each mobile robot is 10 dBm, and its receiving sensitivity is  $-101$  dBm. The center frequency

is set at 3.5 GHz and its bandwidth is 900MHz. All the above parameters are chosen based on actual characteristics of commercial UWB chip DW1000 [29]. In each iteration of the Monte Carlo simulation, different nodes are randomly distributed in the 2-D plane of different sizes. The simulation results are shown in Fig. 10, and the following conclusions could be obtained:

1) *The Maximum Transmission Range:* It is essential to guarantee reliable communication in the robot navigation system. Thus, cooperative mobile robots need to stay connectible to each other within a certain range. The maximum

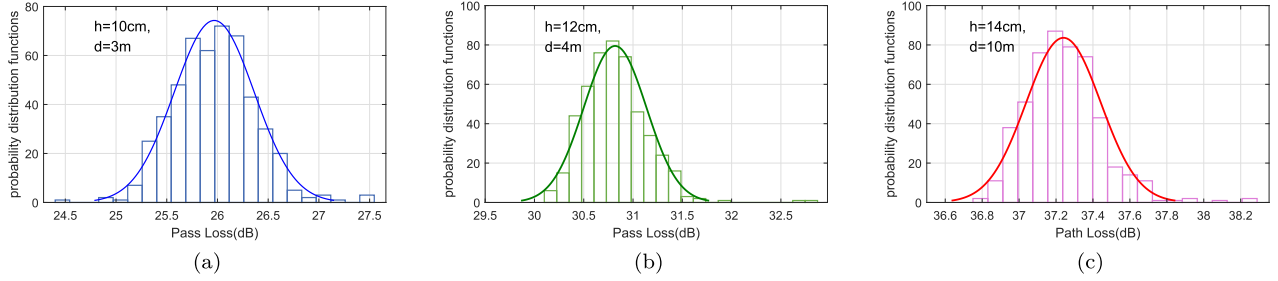


Fig. 11. The path-loss distribution estimated by model on brick floor at different antenna height and distance between Tx and Rx.

transmission range could be found by equating the path-loss and the dynamic range of robots. When path-loss exceeds the dynamic range, the communication between nodes is lost. In Fig. 10-(a), coverage range is evaluated using our proposed two-segmented model with predefined network parameters. The antenna height  $h$  is observed to have a prominent role in confining the coverage area; the maximum transmission range increases obviously when the antenna is elevated from the ground level. Besides, the bigger the maximum dynamic range is, the higher the maximum link range is.

2) *Full Connectivity Probability*: In high-density robot applications, such as unknown environmental monitoring, a large number of low-cost autonomous robots are spatially distributed to cooperatively monitor certain physical or environmental conditions. For each robot, the number of its neighbors has a crucial influence on network performance and reliability. We call it *full connectivity* when each node in the network can communicate with all the others. *Connectivity probability* is defined as the ratio of the number of full connectivity  $N_{fc}$  with a total number in Monte Carlo simulations  $N_s$ . Namely, the full connectivity probability is computed by  $N_{fc}/N_s$ . In our simulation, the number of nodes is respectively set as 60, 40 and 20. The plane size is  $10 \times 10 \text{ m}^2$ . Monte Carlo simulations can provide random network connectivity. From Fig.10-(b) we can see that, the relationship between full connectivity probability and the nodes: the connectivity probability is also related to the antenna height  $h$ . As the number of nodes increases, the full connectivity probability also increases. Furthermore, when the antenna height is higher than 18cm, the full connectivity probability is approaching 1.

3) *The Number of Communicable Neighbors*: In a specific area, node deployment density, that is, the number of communicable nodes, has an important impact on the quality and reliability of near-ground cooperative communication. *The average number of neighbors* is defined as the ratio of total links number within a certain range to the total number of nodes in the network. In Fig.10-(c), the size of experiment area is respectively set as  $100\text{m}^2$ ,  $200\text{m}^2$  and  $300\text{m}^2$ . The total robots number is 30. Given a constant robot number, with the increasing of experiment area, the average number of neighbors generally decrease within a certain antenna height. When the antenna height  $h$  is higher than a certain value, the average number of neighbors retains constant, which indicates that the near-ground condition no more contributes to the communication performance. Besides, when the experiment

area is fixed as  $100\text{m}^2$ , the average number of neighbors shows different performance when the node number is respectively set as 10, 20 and 30. It can be seen that connectivity has high sensitivity to robot antenna height and almost spans the full range as the height increases from the ground level to a specific height. When the antenna is set closer to the ground level, the influence of the antenna height on path-loss is more obvious.

### C. CRLB Analysis of Path-Loss Estimation

CRLB defines the theoretical lower bound of the variance of any unbiased estimator, which is useful as a benchmark to judge estimation methods as well as to evaluate their consistency. It is also generally used to choose optimal parameters in a specific network deployment scenario for reliable communication. For example, in a given application scenario, the antenna needs to be deployed at a specific height of  $h$ . We can calculate CRLB through the proposed model to obtain the desired communication distance  $d$ , to ensure satisfactory communication quality.

In this section, we first derive the closed-form expressions for the CRLB of path-loss based on the proposed two-segmented model as displayed in Equation (22). The proposed channel model is employed to estimate the path-loss in UWB signal transmission.

For a certain sampling point,  $K$  sets of model parameter values can be obtained continuously, and  $K$  path-loss estimated value can be obtained as well, i.e.,  $\hat{PL} = \{\hat{PL}_1, \hat{PL}_2, \dots, \hat{PL}_K\}$ . Based on the least squared fitting method used in Section III, we can get an estimation model for the variance of measured values at each experimental point, namely

$$\begin{aligned}\sigma^2 &= A * d^3 + B * d^2 + C * d + D \\ A &= 2.464 * h^3 + 1.189 * h^2 - 0.19 * h + 0.01015; \\ B &= 68.03 * h^3 - 32.87 * h^2 + 5.255 * h - 0.2796; \\ C &= -553.5 * h^3 + 262.1 * h^2 - 40.94 * h + 2.128; \\ D &= 218.1 * h^3 - 83.5 * h^2 + 9.625 * h - 0.2875;\end{aligned}\quad (24)$$

which indicates that the measuring variance is also closely related to antenna height  $h$  and communication distance  $d$ , and generally follows Gaussian distribution, as shown in Fig. 11.

CRLB of the path-loss estimator can be derived as follows. Path-loss estimators  $\hat{PL}$  conform to Gaussian distribution,

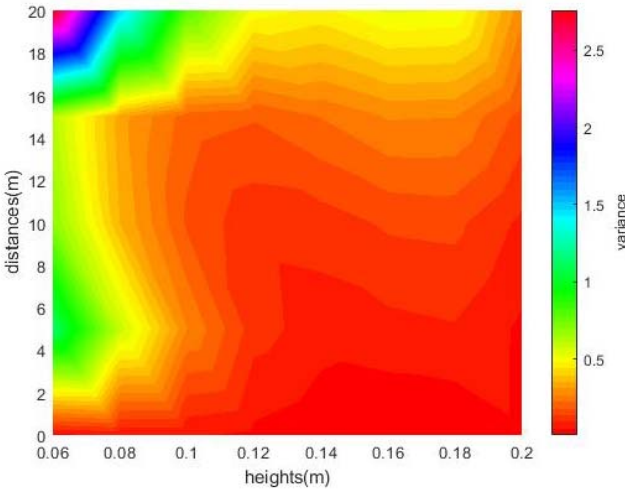


Fig. 12. CRLB calculation for path-loss estimation with different ( $h, d$ ).

that is, each estimator is an unbiased estimator with Gaussian noise:

$$\hat{PL} \in N(\mu, \sigma^2) \quad (25)$$

Thus, the probability distribution function of  $\hat{PL}$  is:

$$f(\hat{PL}) = \frac{1}{\sigma\sqrt{2\pi}} e^{-\frac{(\hat{PL}-\mu)^2}{\sigma^2}} \quad (26)$$

Fisher information matrix (FIM) function [24] is derived as:

$$F = E \left[ \frac{\partial f}{\partial \mu} \right]^2 \quad (27)$$

Then, the CRLB of  $\hat{PL}$  could be represented as:

$$Var[\hat{PL} - PL] \geq F^{-1} = \sigma^2 \quad (28)$$

Based on the above analysis, the relationship between  $\sigma^2$  and  $h, d$  could be calculated and shown as Fig. 12. With close observation, the following results could be achieved:

- Given a certain communication distance  $d$ , with the decrease of antenna height  $h$ , the CRLB increases gradually, which reveals larger bounds and worse estimation performance. This also implies that the possible multi-path condition becomes more serious with lower antenna heights.
- Given a certain antenna height  $h$ , with the increase of communication distance  $d$ , the CRLB gradually increases. However, the antenna height still seems to be the dominant factor on CRLB. Taking  $h = 8cm$  as an example, CRLB with distance from 1 m to 20 m are all beneath 0.85. While  $h = 2cm$ , CRLB could be as large as 2.8.

## V. CONCLUSION

Near-ground condition is an important application scene towards mobile robot navigation. Near-ground channel modeling is very important to ensure efficient and reliable communication between cooperative targets. In this study, we focus on the modeling of near-ground UWB channel, considering the

crucial factors of antenna height, communication distance and surface condition. From both theoretical and practical aspects, we validate the effectiveness of the proposed channel model. The following conclusions could be drawn from the research results of this paper:

- 1) Fresnel zone has an important influence on near-ground channel state, so it is necessary to model it in segments. With comparison experiments, it is proved that the proposed two-segmented model in this paper has a higher estimation accuracy than the traditional empirical model.
- 2) Antenna height, communication distance, and surface environment have different effects on near-ground channel. Within a certain range, the higher the antenna height and the closer the communication distance, the better the communication performance will usually be.

In this study, the influence of terrain roughness on path-loss is statistically analyzed in our models. However, research on theoretical quantification of different surface type on channel signal attenuation characteristics still needs to be explored. This enlightens our future research direction.

## REFERENCES

- [1] M. Chamanbaz *et al.*, "Swarm-enabling technology for multi-robot systems," *Frontiers Robot. AI*, vol. 4, p. 12, Apr. 2017.
- [2] Y. Shen, S. Mazuelas, and M. Z. Win, "Network navigation: Theory and interpretation," *IEEE J. Sel. Areas Commun.*, vol. 30, no. 9, pp. 1823–1834, Oct. 2012.
- [3] M. Z. Win, Y. Shen, and W. Dai, "A theoretical foundation of network localization and navigation," *Proc. IEEE*, vol. 106, no. 7, pp. 1136–1165, Jul. 2018.
- [4] C. J. Hegarty and E. Chatre, "Evolution of the global navigation satellite system (GNSS)," *Proc. IEEE*, vol. 96, no. 12, pp. 1902–1917, Dec. 2008.
- [5] R. Klukas, G. Lachapelle, C. Ma, and G.-I. Jee, "GPS signal fading model for urban centres," *IEE Proc.-Microw., Antennas Propag.*, vol. 150, no. 4, pp. 245–252, 2003.
- [6] J. Pugh and A. Martinoli, "Relative localization and communication module for small-scale multi-robot systems," in *Proc. IEEE Int. Conf. Robot. Automat. (ICRA)*, May 2006, pp. 188–193.
- [7] V. V. Mani and R. Bose, "Direction of arrival estimation of multiple UWB signals," *Wireless Pers. Commun.*, vol. 57, no. 2, pp. 277–289, Mar. 2011.
- [8] K. Guo, Z. Qiu, W. Meng, L. Xie, and R. Teo, "Ultra-wideband based cooperative relative localization algorithm and experiments for multiple unmanned aerial vehicles in GPS denied environments," *Int. J. Micro Air Vehicles*, vol. 9, no. 3, pp. 169–186, Sep. 2017.
- [9] W. M. Merrill, H. L. Liu, J. Leong, K. Sohrabi, and G. J. Pottie, "Quantifying short-range surface-to-surface communications links," *IEEE Antennas Propag. Mag.*, vol. 46, no. 3, pp. 36–46, Jun. 2004.
- [10] A. Torabi and S. A. Zekavat, "Near-ground channel modeling for distributed cooperative communications," *IEEE Trans. Antennas Propag.*, vol. 64, no. 6, pp. 2494–2502, Jun. 2016.
- [11] A. Hugine, H. I. Volos, J. Gaeddert, and R. M. Buehrer, "Measurement and characterization of the near-ground indoor ultra wideband channel," in *Proc. IEEE Wireless Commun. Netw. Conf. (WCNC)*, Apr. 2006, pp. 1062–1067.
- [12] S. Sangodoyin, S. Niranjayan, and A. F. Molisch, "Ultrawideband near-ground outdoor propagation channel measurements and modeling," in *Proc. 7th Eur. Conf. Antennas Propag. (EuCAP)*, Apr. 2013, pp. 3034–3038.
- [13] W. Khawaja, I. Guvenc, and D. Matolak, "UWB channel sounding and modeling for UAV air-to-ground propagation channels," in *Proc. IEEE Global Commun. Conf. (GLOBECOM)*, Dec. 2016, pp. 1–7.
- [14] H. Klaina, A. V. Alejos, O. Aghzout, and F. Falcone, "Narrowband characterization of near-ground radio channel for wireless sensors networks at 5G-IoT bands," *Sensors*, vol. 18, no. 8, p. 2428, 2428.
- [15] A. F. Molisch, "Ultrawideband propagation channels-theory, measurement, and modeling," *IEEE Trans. Veh. Technol.*, vol. 54, no. 5, pp. 1528–1545, Sep. 2005.

- [16] E. F. Lee and C. Wang, "A study of radio signal behaviors in complex environments," Dept. Comput. Sci., Michigan State University, East Lansing, MI, USA, Tech. Rep. MSU-CSE-06-6, 2006. Accessed: Jul. 15, 2018. [Online]. Available: <http://www.cse.msu.edu/publications/tech/TR/MSU-CSE-06-6.pdf>
- [17] J. R. Hampton, N. M. Merheb, W. L. Lain, D. E. Paunil, R. M. Shuford, and W. T. Kasch, "Urban propagation measurements for ground based communication in the military UHF band," *IEEE Trans. Antennas Propag.*, vol. 54, no. 2, pp. 644–654, Feb. 2006.
- [18] G. G. Joshi *et al.*, "Near-ground channel measurements over line-of-sight and forested paths," *IEE Proc.-Microw., Antennas Propag.*, vol. 152, no. 6, pp. 589–596, 2005.
- [19] M. Rodriguez, R. Feick, H. Carrasco, R. Valenzuela, M. Derpich, and L. Ahumada, "Wireless access channels with near-ground level antennas," *IEEE Trans. Wireless Commun.*, vol. 11, no. 6, pp. 2204–2211, Jun. 2012.
- [20] J. Zang and X. Wang, "Measurements and modeling of path loss over irregular terrain for near-ground and short-range communications," *Prog. Electromagn. Res.*, vol. 57, pp. 55–62, Jan. 2017.
- [21] T. Tokunou, R. Yamane, and T. Hamasaki, "Near earth propagation loss model in forest for low power wireless sensor network," in *Proc. USNC-USRI Radio Sci. Meeting*, San Diego, CA, USA, Jul. 2017, pp. 19–20.
- [22] W. Khawaja, K. Sasaoka, and I. Guvenc, "UWB radar for indoor detection and ranging of moving objects: An experimental study," in *Proc. Int. Workshop Antenna Technol. (iWAT)*, 2016, pp. 102–105.
- [23] Accessed: Apr. 15, 2020. [Online]. Available: <https://github.com/sakai3/data-for-UWB.git>
- [24] C. Xu, J. He, X. Zhang, P.-H. Tseng, and S. Duan, "Toward near-ground localization: Modeling and applications for TOA ranging error," *IEEE Trans. Antennas Propag.*, vol. 65, no. 10, pp. 5658–5662, Oct. 2017.
- [25] M. H. Hebert, C. E. Thorpe, and A. Stentz, Eds., *Intelligent Unmanned Ground Vehicles: Autonomous Navigation Research at Carnegie Mellon*, vol. 388. Springer, 2012.
- [26] F. Qian *et al.*, "Ground robotic measurement of aeolian processes," *Aeolian Res.*, vol. 27, pp. 1–11, Aug. 2017.
- [27] K. R. Aravind, P. Raja, and M. Pérez-Ruiz, "Task-based agricultural mobile robots in arable farming: A review," *Spanish J. Agricult. Res.*, vol. 15, no. 1, pp. 1–16, 2017.
- [28] J. Ahmadi, "The effects of Fresnel zone in communication theory based on radio waves," *Bull. la Soc. Royale Sci. Liège*, vol. 85, pp. 729–734, Jan. 2016.
- [29] *DW1000 Datasheet. Version 2.12*. Decawave Ltd., Dublin, Ireland, 2016.
- [30] S. Netrapala, "Statistical analysis of indoor UWB channel parameters in different wall corridors and through-wall environments," Univ. Texas Arlington, Arlington, TX, USA, Tech. Rep., 2015.
- [31] K. S. Bangalore, "Channel estimation and statistical analysis of indoor environment using ultrawideband radio technology," Univ. Texas Arlington, Arlington, TX, USA, Tech. Rep., 2015.
- [32] K. Y. Kapusuz and A. Kara, "Determination of scattering center of multipath signals using geometric optics and fresnel zone concepts," *Eng. Sci. Technol., Int. J.*, vol. 17, no. 2, pp. 50–57, Jun. 2014.
- [33] M. Grimm and D. Manteuffel, "Norton surface waves in the scope of body area networks," *IEEE Trans. Antennas Propag.*, vol. 62, no. 5, pp. 2616–2623, May 2014.
- [34] K. A. Norton, "The calculation of ground-wave field intensity over a finitely conducting spherical Earth," *Proc. IRE*, vol. 29, no. 12, pp. 623–639, Dec. 1941.
- [35] *Decawave Channel Technique Report*. Accessed: Jan. 19, 2020. [Online]. Available: [https://www.decawave.com/wp-content/uploads/2018/12/Comparison-of-Narrowband-and-Ultra-Wideband-Channels\\_2018-01-04.pdf](https://www.decawave.com/wp-content/uploads/2018/12/Comparison-of-Narrowband-and-Ultra-Wideband-Channels_2018-01-04.pdf)



**Shihong Duan** received the M.S. and Ph.D. degrees in pattern recognition and computer science from the University of Science and Technology Beijing (USTB), China, in 1998 and 2012, respectively. Since July 2013, she has been an Associate Professor with the School of Computer and Communication Engineering, USTB. From August 2014 to August 2015, she was a Visiting Scholar with the Center for Wireless Information Network Studies, Worcester Polytechnic Institute. Her research interests include swarm intelligence, mobile computing, and pattern recognition.



**Ran Su** is currently pursuing the bachelor's degree in computer science and technology with the University of Science and Technology Beijing (USTB). He shows a great interest in algorithm design and big data digging.



**Cheng Xu** (Member, IEEE) received the B.E., M.S., and Ph.D. degrees from the University of Science and Technology Beijing (USTB), China, in 2012, 2015, and 2019, respectively. He is currently working as an Associate Professor with the Data and Cyber-Physical System Lab (DCPS), University of Science and Technology Beijing. He is supported by the Post-doctoral Innovative Talent Support Program from Chinese government in 2019. His research interests now include swarm intelligence, multirobots networks, wireless localization, and the Internet of things. He is an Associate Editor of *International Journal of Wireless Information Networks*.



**Yulin Chen** received the bachelor's degree in civil engineering from the University of Science and Technology Beijing (USTB) in 2018, where he is currently pursuing the Ph.D. degree in computer technology. His research interests are in swarm intelligence and multiagents system, with a focus on consensus algorithms.



**Jie He** received the B.E. and Ph.D. degrees in computer science from the University of Science and Technology Beijing (USTB), China, in 2005 and 2012, respectively. Since July 2015, he has been an Associate Professor with the School of Computer and Communication Engineering, USTB. From April 2011 to April 2012, he was a Visiting Ph.D. Student with the Center for Wireless Information Network Studies, Worcester Polytechnic Institute. His research interests include wireless indoor positioning, human gesture recognition, and motion capture.